# THEORETICAL FOUNDATIONS OF CIVIL ENGINEERING

## VOLUME VII

## STRUCTURAL MECHANICS


Edited by
Stanisław Jemioło
and Marcin Gajewski

Warsaw 2016

MONOGRAPHS OF FACULTY OF CIVIL ENGINEERING

# XI COHESIVE ELEMENT APPROACH FOR DETERMINATION OF MASONRY PANELS LIMIT STATES

*Łukasz KOWALEWSKI, Marcin GAJEWSKI*

## 1. Introduction

Typical unreinforced masonry structures are made by joining bricks with mortar [2, 6, 9]. The effective properties of elasticity and plasticity in macroscopic models are determined by brick layout, as well as the mechanical parameters of bricks and mortar [9]. Experiments carried out on brickwork panels confirm that before reaching failure state the wall elements treated as a whole present features of elastic anisotropy (in particular orthotropy) [11, 12]. On the other hand, failure state is usually determined by a brittle cracking of bed joints in a tension mode [5]. In general brick cracking and crushing in so called compression mode occurs only in exceptional cases [2]. As a consequence of these observations it is clear that in macroscopic modeling in the elastic range the orthotropic generalized Hooke's relationship is needed [8]. Also transition to the limit state of the brickwork is determined with pressure insensitive (understood as a dependence on the trace of the stress tensor) or pressure sensitive orthotropic yield conditions like Hill's in first case and Hoffmann's [6] in the second one.

Studies carried out in this chapter are connected with analysis of the failure mechanisms in relatively thin (modeled with plane stress assumption) masonry panels, subjected to the biaxial stress state, taking into account an angle between bed joint plane and loading axis (principal stress directions). The so called micro-modeling approach is used, meaning that each component of masonry wall can be distinguished (for wider view on different modeling strategies see [8]).The bricks are modeled with linear elasticity constitutive model for isotropic materials, whilst to model the interface (mortar) the cohesive elements [3], with elasto-plasticity constitutive relationship that allows to describe fracture and post-critical weakening, are used (see [5]).

As a background for presentation of obtained numerical results the original research carried out by Page in the 80's is used [13, 14]. The results of numerical tests on Page's masonry panels, modeled using ABAQUS software and constitutive relations shown in section 2, are presented in section 3. Having results of Page's experimental tests [13, 14] it is possible to evaluate the applied numerical approach and to specify the limits of its applicability. The general conclusion from these analysis is that in cases where the panels are compressed in one direction (without tensioning in perpendicular direction) there is no

strength limitation in a constitutive modelling of constituent materials. The first step in the problem solution is a proposition of the yield condition for the brick material. Having in mind that brick-panels are modeled with plane stress assumption even the Huber-Mises yield condition can be applied after adjusting to the proper experimental tests. Such condition give a limitation for stresses in compression mode, but its limitations in tension mode (obviously too high compared to the real material properties) are not going to be met because the tension condition in mortar will have been activated long before. Such supplemented constitutive model is applied for the solution of the brick-wall crushing test presented in section 4 proving its usefulness.

It is worth to underline here that this chapter is an extended and rewritten version of the conference paper [7]. So the numerical solutions of biaxial compression-tension tests in a more detailed form are presented here again. The new and original part of this chapter is a presentation of the simple recipe to solve one of the main disadvantages of the modeling approach presented in [7]. This disadvantage was identified in a problems where brick-panels are under compression, in such cases there is no failure criteria in the constitutive model to limit compression strength of a brick-panel.

## 2. Constitutive modelling of heterogeneous masonry structures

### 2.1. Constitutive model for bricks

To describe the elastic behavior of bricks the linear Hooke's relationship for isotropic materials is assumed:

$$\boldsymbol{\sigma} = \frac{\nu E}{(1-2\nu)(1+\nu)}(\mathrm{tr}\boldsymbol{\varepsilon})\mathbf{I} + \frac{E}{(1+\nu)}\boldsymbol{\varepsilon}, \tag{2.1}$$

where $\boldsymbol{\sigma}$ and $\boldsymbol{\varepsilon}$ are respectively stress and strain symmetrical second order tensors, $\mathbf{I}$ is an identity second order tensor and „tr" is a tensor trace operator.

### 2.2. Constitutive model of an interface

Before the failure occur, interface material (mortar) is working as a linear elastic material, with the constitutive relationship between the interface stress vector $\mathbf{t}$ ($\mathbf{t}=\boldsymbol{\sigma}\mathbf{n}$, where $\mathbf{n}$ is a normal to the interface plane vector, and $\boldsymbol{\sigma}$ is a stress tensor outside the interface) and strain vector $\hat{\boldsymbol{\varepsilon}}$ in the following form:

$$\mathbf{t} = \mathbf{K}\hat{\boldsymbol{\varepsilon}} \rightarrow t_i = K_{ij}\hat{\varepsilon}_j, \quad \text{where } i,j = \mathrm{n,s,t} \tag{2.2}$$

where $\mathbf{K}$ is a second order tensor describing interface stiffness. The indexes for $\mathbf{K}$ components can be interpreted according to Fig.2.1. In the relationship "n" stands for the direction normal to the interface plane and "t", "s" describe two directions perpendicular to each other and laying in the interface plane. The relationship in the form (2.2) allows taking into account an anisotropic elastic properties of the interface for tension/compression and shearing modes of deformations. In (2.2) $\hat{\boldsymbol{\varepsilon}}$ is a nominal strain vector, with components defined like below:

$$\varepsilon_i = \frac{\delta_i}{T_0}. \tag{2.3}$$

In (2.3), $\delta_i$ are interpreted as the displacements in interface, and $T_0$ is the interface initial thickness.

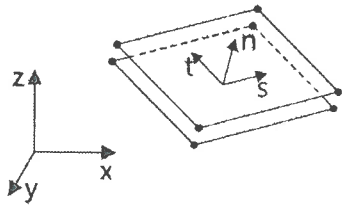


**Figure 2.1.** Local coordinate system in cohesive elements.

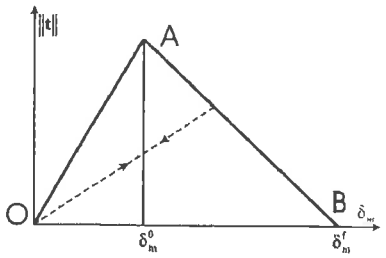


**Figure 2.2.** Degradation of the interface stiffness after failure initiation.

There is a range of deformation when the interface is working as linearly-elastic, cf. Fig.2.2, but after crossing a failure criterion expressed in terms of stresses or strains the stiffness of the joint is decreasing and finally becomes equal to zero. When the joint stiffness is zero the permanent deformations occur. As a failure criterion the following condition in the form of quadratic function with respect to the stress vector components may be assumed:

$$F(t_i)=\left(\frac{\langle t_n\rangle}{t_n^{\max}}\right)^2+\left(\frac{t_s}{t_s^{\max}}\right)^2+\left(\frac{t_t}{t_t^{\max}}\right)^2\le 1,$$
$$\langle t_n\rangle=\begin{cases}t_n, & t_n\ge 0\\ 0, & t_n<0\end{cases}. \tag{2.4}$$

As it is clear from the lower (2.4) formula the condition is not sensitive to pure compression in "n" direction. Similar condition to (2.4) can be written in the strain vector space as well, cf. [7]. In the numerical tests presented below, the failure criterion depending on stresses in the form (2.4) is applied. In (2.4) the three interface stress vector components are present, while $t_i^{\max}$ are maximum values of these vector components, determined in the uniaxial tension test and shearing tests conducted in two perpendicular directions (Fig.2.1). In the presented model (cf.[1]) the real stress vector components are derived with the following equations:

$$\begin{aligned}t_n&=(1-D)\langle\bar{t}_n\rangle,\\ t_s&=(1-D)\bar{t}_s,\\ t_t&=(1-D)\bar{t}_t,\end{aligned} \tag{2.5}$$

where $\bar{t}_i$ are stress vector components derived from (2.2) with the assumption that the failure condition is not met. A scalar parameter $D$ (degradation) depends linearly or exponentially on maximum strains achieved in the interface. Aforementioned linear relationship can be written in the following form:

$$D=\frac{\delta_m^f\left(\delta_m^{\max}-\delta_m^0\right)}{\delta_m^{\max}\left(\delta_m^f-\delta_m^0\right)}, \tag{2.6}$$

while exponential one is quite more complicated and can be found in [7]. In expression (2.6) parameter $\delta_m$ is defined as

$$\delta_m=\sqrt{\langle\delta_n\rangle^2+\delta_t^2+\delta_s^2} \tag{2.7}$$

Graphical interpretation of the $\delta_m^f$ and $\delta_m^0$ parameters can be found in Fig.2.2. The parameter $\delta_m^{\max}$ describes maximum value of the displacement in the interface during the entire loading history and $\delta_m^{\max} \in [\delta_m^0, \delta_m^f]$. As a result $D$ parameter is modified for $\delta_m > \delta_m^0$ ,it is constant during material unloading and its value is always from the interval: $D \in [0,1]$ (if $D=0$ there is no degradation of elastic properties, if $D=1$ there is no interface stiffness, interpreted as full degradation). A detailed description of this model can be found, among others, at [3].

## 3. Numerical tests – masonry panels biaxial tension/compression tests

### 3.1. Material data

Material parameters in constitutive relationships presented in section 2 for both brick and mortar were assumed as in works [9, 11, 13], therefore the comparison of numerical test results with results of Page's studies can only be analyzed on the qualitative level. Summary of all material data is given in Tab.3.1.

**Table 3.1.** Material properties for bricks and mortar interface.

| Bricks | | Interface | | | | |
|---|---|---|---|---|---|---|
| $E$ $[N/mm^2]$ | $\nu$ | $K_{nn}$ $[N/mm^2]$ | $K_{ss}$ $[N/mm^2]$ | $t_n^{\max}$ $[N/mm^2]$ | $t_s^{\max}$ $[N/mm^2]$ | $\delta_m^f$ $[mm]$ |
| 20000 | 0.15 | 2000 | 890 | 0.5 | 0.75 | 0.08 |

In the case of adopted cohesive elements a simplified constitutive relationship is applied - in (2.3) the only non-zero components are present on the diagonal. It should also be noted that the constitutive relationship described in section 2.2 for the interface does not include material damage as a result of compression, but still it is highly non-linear [15].

### 3.2. Models for numerical tests

To resemble the experimental tests presented in works [4, 14, 15] the four FEM models of square panels were created, measuring 665 x 665 mm, with directions of bed joints (global principal orthotrophy directions) inclined to x axis with 0.0°, 22.5°, 45° and 67.5° angle respectively, cf. Fig.3.2. The brickwork layout and dimensions of bricks, joints and panels are adopted analogous to those presented in Page's work [14].

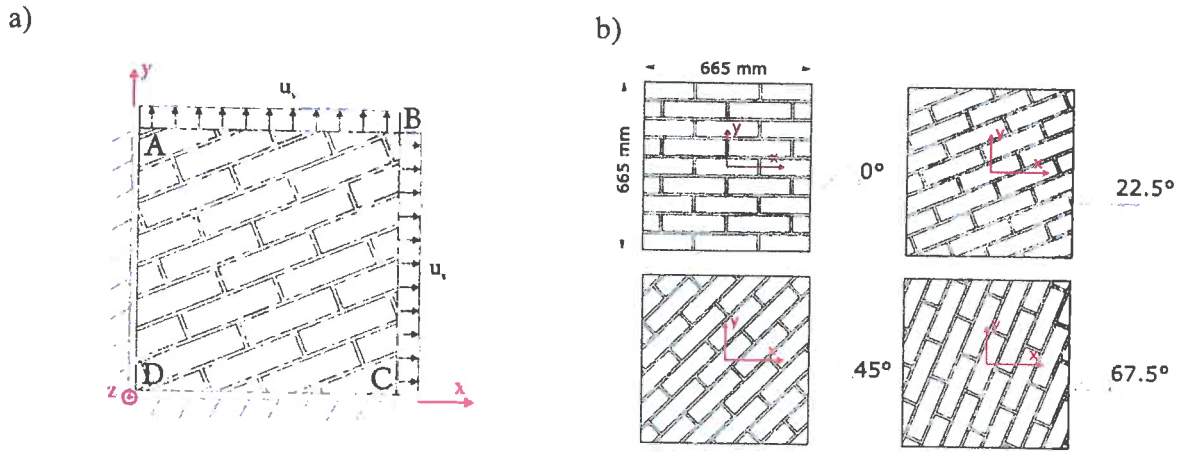


**Figure 3.1.** Masonry test panels: a) displacement and stress type boundary conditions, b) bed joints orientation with respect to x axis.

In every analyzed case on two edges perpendicular to each other (e.g. AD and CD, Fig. 4a) the zero displacement boundary conditions were assumed, while in nodes laying on AB and BC edges (boundaries) the displacement were assumed realizing compression/tension in x and y direction respectively. For each boundary condition configuration four numerical tests were performed on each panel using finite element system ABAQUS [1].

The main objective of the work presented here was to determine the limit surface for biaxial compression-tension tests considering different orientation of the bed joints. The uniaxial strain test was conducted first, by controlling the vertical displacement in nodes of the upper AB edge of the panel, and blocking the horizontal displacements of the nodes on edges AD and BC. Numerical solution of the following tasks was divided into two steps-in the first one the displacements in direction x (on edge BC) were applied, resulting in a uniaxial strain compression. In the first step of analysis, (in most cases) all the components of the panel worked within elasticity range. In the second step, the displacements in y direction of the nodes of the upper edge of the panel were forced, causing tension and eventually the failure of the panel. In subsequent tests, in the nodes on the BC edge the values of displacements in the x direction were increased to: 0.05, 0.10, and 0.15 [mm] respectively, changing the values of effective (average) horizontal stresses.

All the results presented below were calculated for 2D models in plane stress case. To model the bricks the CPS4R and CPS3R elements were used (four or three node, bilinear elements with reduced integration). In case of mortar modeling the 2D, four node, linear, cohesive elements (COH2D4) were applied. In Fig. 3.1 the FEM meshes are presented showing different orientation of the bed joints direction (a - 0.0°, b - 22.5°, c - 45° and d - 67.5°) with respect to the x axis. In first case mesh consist of 4067 elements CPS4R type and 690 elements COH2D4 type, for 22.5° - 4118 CPS4R, 742 COH2D4 and 108 CPS3, for 45°:4185CPS4R, 734COH2D4 and 126 CPS3, and for 67.5°: 4100 CPS4R, 743 COH2D4 and 72 CPS3 elements. In general the bed joints are modeled with one cohesive element through the thickness of a joint, and brick is modeled with about 7 elements through its thickness. The automatic mesh generator was applied, so in some cases also three node elements were generated.

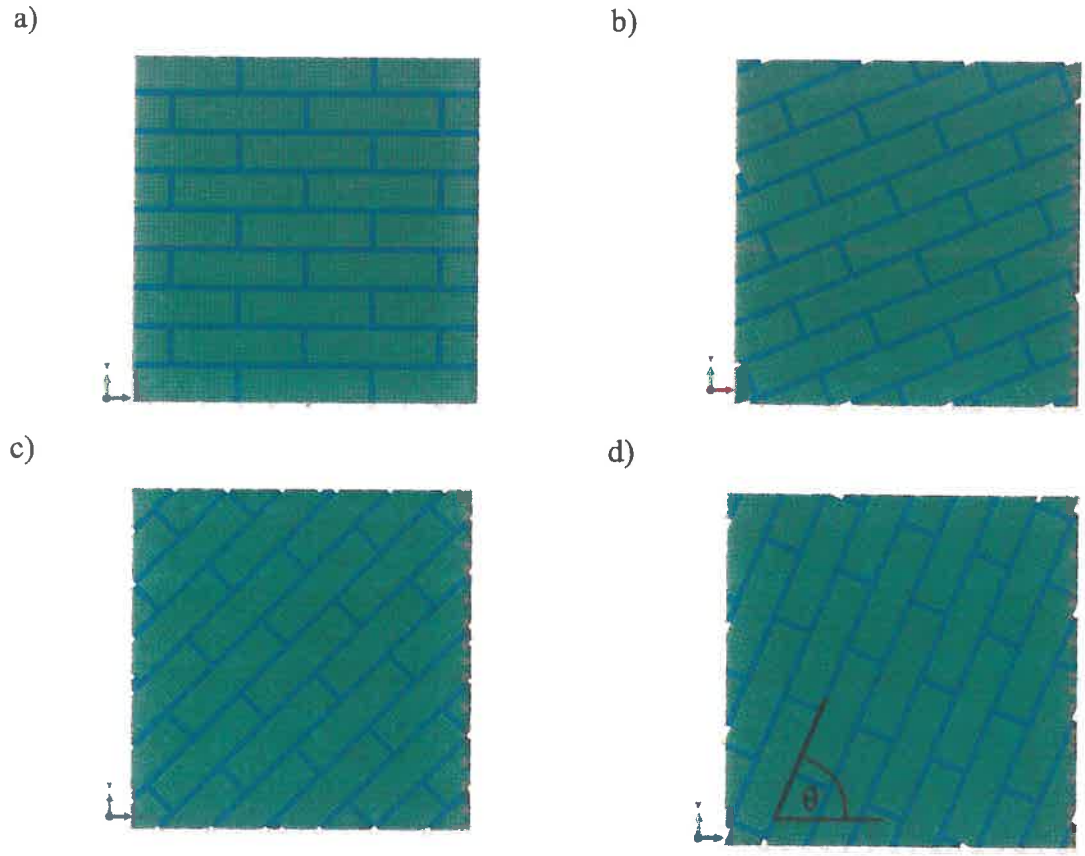


**Figure 3.2.** FEM meshes with global coordinate system generated for different value of $\theta$ angle.

### 3.3. Analysis of numerical test results

Table 3.2 summarizes the results of brickwork compression/tension load capacity tests. For each assumed displacement value $u_x$ leading to compression in x direction the sum of respective reaction forces in corresponding nodes was read, based on which the average effective compressive stress $\sigma_{xx}$ was calculated. On the other hand, the stress component $\sigma_{yy}$ is the average value of maximal tensile stress that the panel carries, and was calculated as the sum of reaction forces of nodes with boundary conditions $u_y$ applied, divided by the initial cross-section area.

Based on the tests results the failure surface was created, wherein the additional axis indicates the angle of rotation of the bed joints of the panel in relation to the direction of the principal stresses (compressive force direction) (see [13, 14]).

Values in bold denote the average normal stress in the y direction interpreted as average yield strength, while $\sigma_{xx}$ is the value of the average normal stress in the x direction, which appears after applying the initial displacement $u_x$. In case of compressive loading at an angle of 0.0° or 90.0° the failure of the panels did never occur, due to adopted constitutive relationships, which do not allow for the occurrence of a compressive failure.

**Table 3.2.** Ultimate stresses in compression-tension tests.

| | 0.0° | | 22.5° | | 45.0° | | 67.5° | | 90.0° | |
|---|---|---|---|---|---|---|---|---|---|---|
| $u_x$ | $\lvert\sigma_{xx}\rvert$ | $\sigma_{yy}$ | $\lvert\sigma_{xx}\rvert$ | $\sigma_{yy}$ | $\lvert\sigma_{xx}\rvert$ | $\sigma_{yy}$ | $\lvert\sigma_{xx}\rvert$ | $\sigma_{yy}$ | $\lvert\sigma_{xx}\rvert$ | $\sigma_{yy}$ |
| *[mm]* | *[N/mm²]* | | | | | | | | | |
| -0.00 | 0 | **0.485** | 0 | **0.515**[iii] | 0 | **0.659**[i] | 0 | **0.794**[iv] | 0 | **1.178** |
| -0.05 | 1.041 | **0.476** | 0.860 | **0.466** | 0.682 | **0.761** | 0.644 | **0.808** | 0.704 | **1.189** |
| -0.10 | 2.082 | **0.455** | 1.698 | **0.272** | 1.314 | **0.137**[ii] | 1.288 | **0.616** | 1.408 | **1.187** |
| -0.15 | 3.123 | **0.425** | **1.797** | **~0** | **1.317** | **~0** | **1.851** | **~0** | 2.113 | **1.184** |

The main result of conducted numerical tests is presented in Fig. 3.3, as a graphical representation of Tab.3.2. The graph shows the dependence of the in-plane masonry panel failure surface on the angle of the load applied. It is a 3D surface for compression/tension tests obtained analogically to that presented in Page [13, 14] for biaxial compression/compression or compression/tension experimental tests. It is clearly visible that the nature of the resulting surface (with the accuracy to the adopted constitutive relations) corresponds to the behavior of real masonry panels.

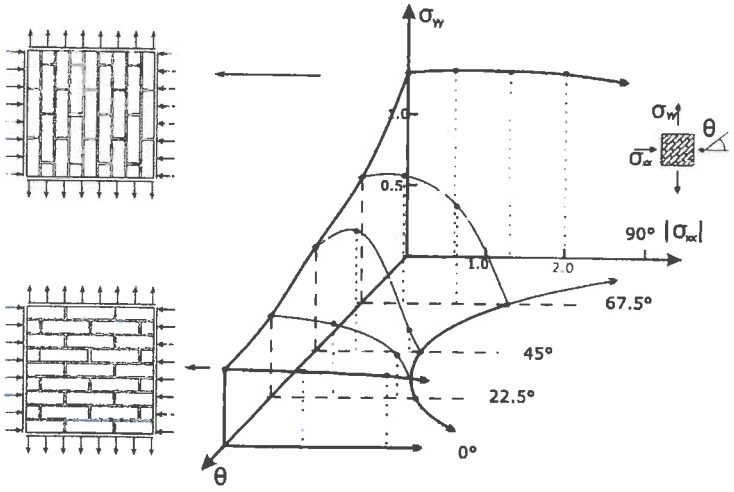


**Figure 3.3.** Failure surface for the biaxial compression/tension obtained from numerical tests.

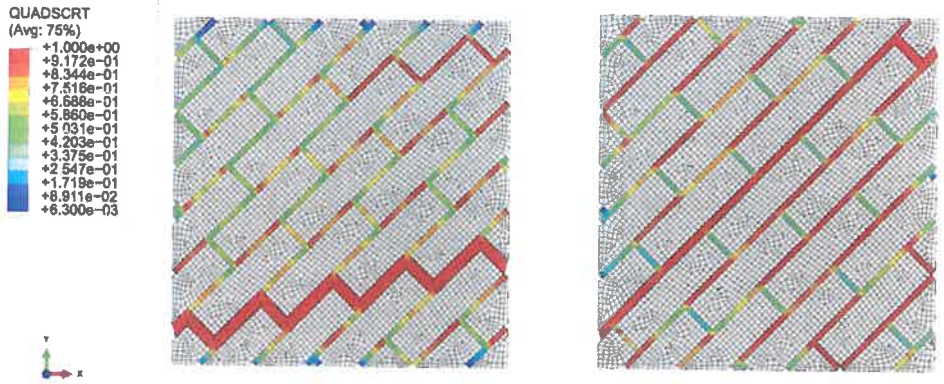


**Figure 3.4.** Panel failure mode for $\theta = 45.0^{o}$ with: a) no initial compression in x direction (marked "i" in Table 3.2), b) 0.1 mm initial compression in x direction (marked "ii"). The quantity QUADSCRT is interpreted as $F(t_i)$, see equation (2.4).

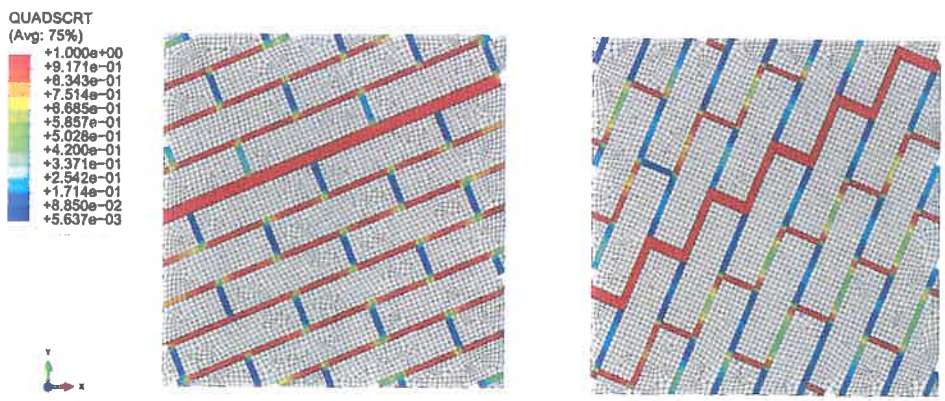


**Figure 3.5.** Panel failure mode for: a) $\theta = 22.5^{o}$ (marked "iii" in table 3.2), b) $\theta = 67.5^{o}$ panel ("iv").

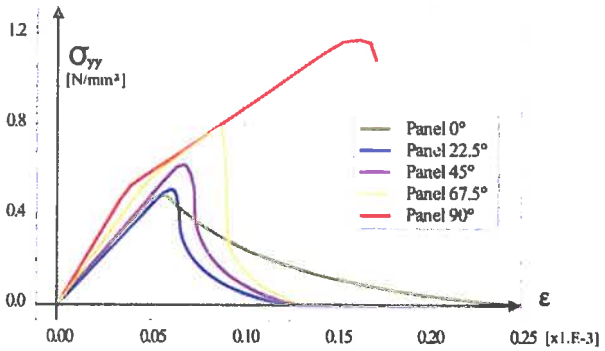


**Figure 3.6.** Comparison of stress-strain relationship for different panels in tests with no initial compression ($\sigma_{xx} = 0$).

The failure mode of the brickwork panels (in case of $\theta = 45.0^{o}$) is presented in Fig. 3.4. The contour graph shows the value of the left side of the failure condition (2.4) in the cohesive elements. Fig. 3.4a shows the failure mode for the tensile test with no initial compression in the x direction applied, whereas in the test the result of which is shown in Fig. 3.4b the value of initially forced displacement $u_x$ was greater than 0. In the latter case slip occurred alongside bed joint in which initial compression caused shear stress of maximal value. Both cases show that failure mode in such masonry panel is dependent not only on the geometry (bricks layout) or the direction of the tensile load, but also on the occurrence of shear stresses in interface (mortar).

In Fig. 3.5 the comparison of failure modes of the panels with $\theta = 22.5^{o}$ and $\theta = 67.5^{o}$ with no initial compression is shown. Finally, Fig. 3.6 shows a comparison of functions of averaged stress versus strain for various values of the $\theta$ angle of the tensile tests in the y direction with no compressive stresses in the x direction. In the case of significant angle value in between the bed joint and the x direction (in Fig. 3.4a, $\theta = 67.5^{o}$ and $\theta = 90.0^{o}$) the phenomenon of sudden change in the effective stiffness of the panel, due to the faster failure of head joints under tension than shearing failure of the bed joints, can be observed. From the theory of plasticity point of view the observed phenomenon can be interpreted as so called stress redistribution in the brickwork element [10].

## 4. Modification of constitutive model for bricks

As it was mentioned above, modeling of the brick material as an elastic one only, in some loading cases, may lead to misinterpretations, as the constitutive model for cohesive interface presented in subsection 2.2 does not consider compressive failure in the material. To overcome this, a simple plasticity criterion was taken into account when modeling brickwork behavior in.

Of course the yield condition for a brittle cracking materials (like brick) should depend on the first stress invariant (average pressure), for example Coulomb-Mohr (CM) or Drucker-Prager criteria, cf. [10, 11]. Still it is proposed to use Huber-Mises-Hencky yield criterion (insensitive to first stress invariant) due to its simplicity and because, when reduced to the 2D model (plane stress case), H-M-H criterion can be matched with CM criterion with respect to biaxial and uniaxial compressive strength of the material, cf. Fig. 4.1a. The HMH yield function can be written in the following form [10]:

$$F\left(\boldsymbol{\sigma},\bar{\varepsilon}^{pl}\right)=f(\boldsymbol{\sigma})-\sigma_{p}\left(\bar{\varepsilon}^{pl}\right). \tag{4.1}$$

where $\sigma_{p}\left(\bar{\varepsilon}^{pl}\right)$ (of course $\sigma_{p}(0)=\sigma_{0}$) is a stress function in the uniaxial (tension/compression) test and $\bar{\varepsilon}^{pl}$ is an equivalent plastic strain. By defining the function $\sigma_{p}\left(\bar{\varepsilon}^{pl}\right)$ it is possible to characterize isotropic strain hardening/softening of the material. Such function can be determined on the basis of the uniaxial tension/compression test which exemplary results for a typical quasi-brittle material are presented in Fig. 4.1b. The H-M-H plastic flow potential have the form

$$f(\boldsymbol{\sigma})=\sqrt{\frac{2}{3}\mathbf{s}.\mathbf{s}}, \tag{4.2}$$

where $\mathbf{s}$ is the deviator of stress tensor ($\mathbf{s}=\boldsymbol{\sigma}-(\mathrm{tr}\boldsymbol{\sigma})\mathbf{I}/3$) and the operator in between deviators denoted with "dot" is a full contraction operator.

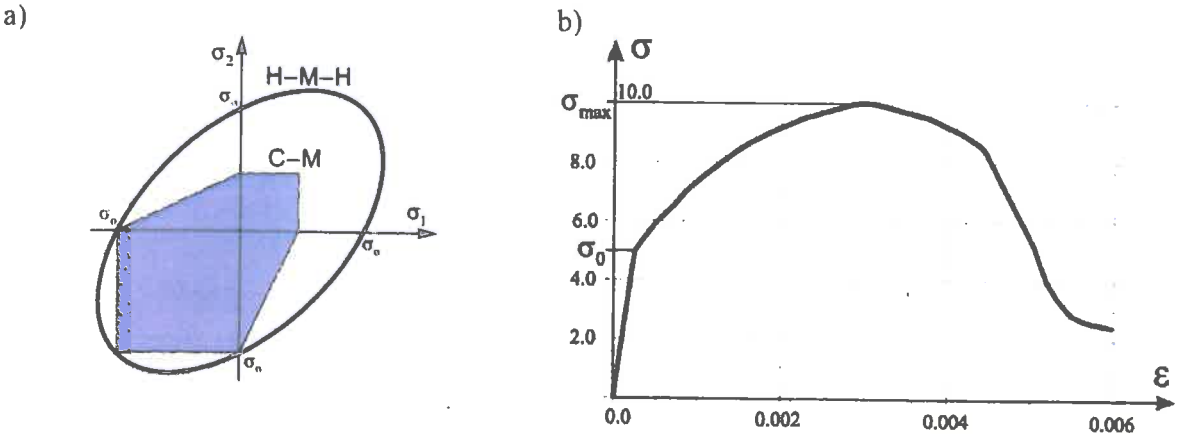


**Figure 4.1.** a) Comparison of H-M-H with Coulomb-Mohr surface in $\sigma_{3}=0$ plane, b) stress- strain relationship for the modified brick material.

### 4.1. Panels biaxial tension/compression tests taking into account plasticity for bricks

After the addition of plasticity to brick material constitutive relation, the numerical tests, corresponding to cases where compression was significant, were updated. In the first attempt the compressive strength of brick was set to $\sigma_{max}$=20 MPa whilst the initiation of plastic flow was taking place around $\sigma_0$=10 MPa. Such assumption is closer to the real brick material behavior, but the overall strength of the masonry wall would be overestimated. In order to obtain the ultimate load values closer to Page's work, the stress - strain relationship in the brick material was taken as it is shown in Fig 4.1, with $\sigma_{max}$=10 MPa compressive strength and $\sigma_0$=5 MPa beginning of yield. However, even with reduced strength of brick material, the inclusion of plasticity did not influence most of the results of previous tests - compressive displacement larger than 0.15 mm was required to reach the limit value of 5 MPa in any of the bricks, and in panels 22.5°, 45.0° and 67.5° such displacement caused failure of mortar interface. The results of updated tests for panels 0.0° and 90.0° are presented below for both cases of brick compressive strength, cf. Tab 4.1 and Fig. 4.2.

**Table 4.1.** Ultimate stresses in compression-tension tests taking into account plasticity in bricks modelling.

| | $\sigma_0$=5[N/mm²], $\sigma_{max}$=10[N/mm²] | | | | $\sigma_0$=10[N/mm²], $\sigma_{max}$=20[N/mm²] | | | |
|---|---|---|---|---|---|---|---|---|
| | 0.0° | | 90.0° | | 0.0° | | 90.0° | |
| $u_3$ | $\lvert\sigma_{xx}\rvert$ | $\sigma_{yy}$ | $\lvert\sigma_{xx}\rvert$ | $\sigma_{yy}$ | $\lvert\sigma_{xx}\rvert$ | $\sigma_{yy}$ | $\lvert\sigma_{xx}\rvert$ | $\sigma_{yy}$ |
| [mm] | [N/mm²] | | | | | | | |
| -0.50 | 5.381 | **0.421** | 4.843 | **1.020** | 8.97 | **0.335** | 6.99 | **1.14** |
| -1.00 | 7.044 | **0.435** | 6.855 | **0.949** | 12.59 | **0.261** | 11.37 | **0.949** |
| -1.50 | 8.053 | **0.441** | 9.225 | **~0** | - | - | - | - |
| -2.00 | 9.662 | **~0** | - | - | 16.59 | **0.269** | 16.55 | **0.529** |
| -3.00 | - | - | - | - | 17.00 | **~0** | 17.00 | **~0** |

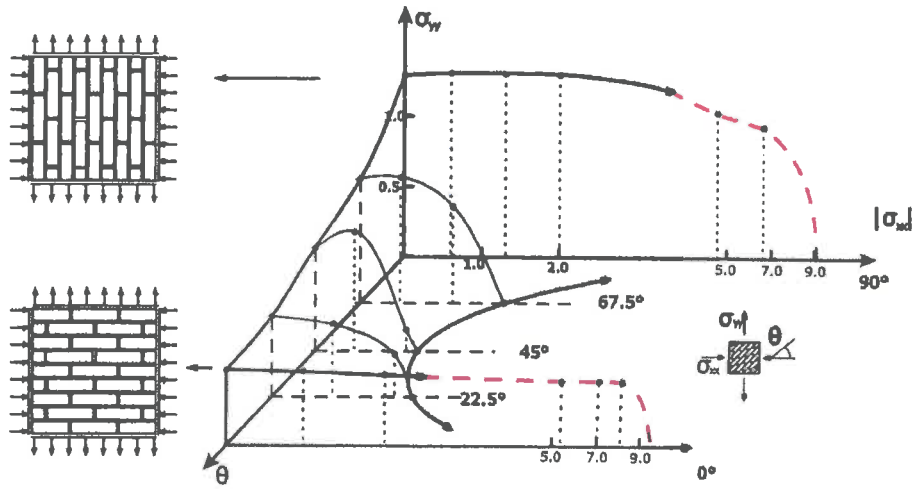


**Figure 4.2.** Updated failure surface for the biaxial compression/tension (plasticity characteristic values $\sigma_0$=5 [N/mm²], $\sigma_{max}$=10 [N/mm²]).

Fig 4.3 shows the updated failure surface for the first case of the strength of brick material (10 MPa strength).

### 4.2. Masonry wall crushing test

Using brick material constitutive relation that supports compressive failure the test of masonry wall crushing was carried out. Isotropic hardening parameters were taken as in previous point (Fig 4.1b) with 10 MPa compressive strength. The wall is 8 bricks wide, 9 bricks high, made from the same elements as the analyzed panels and with the same bricks layout. The boundary conditions assumed for the model can be seen in Fig 4.4. Along the boundary AF the zero displacement boundary conditions were applied while along AB, BC, DF, and EF the zero stress boundary conditions are assumed. Loading of the wall is assumed through displacement boundary conditions on the boundary CD (uniform along CD, vertical displacement with direction to the wall base is applied).

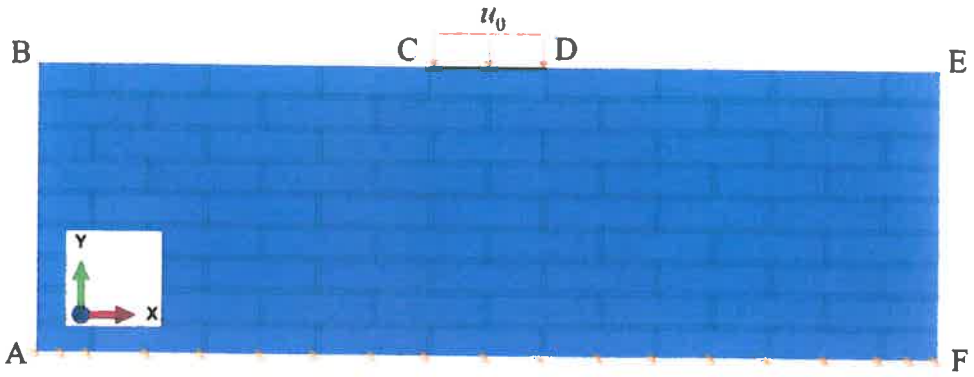


**Figure 4.3.** Boundary conditions for the brick-wall crushing test.

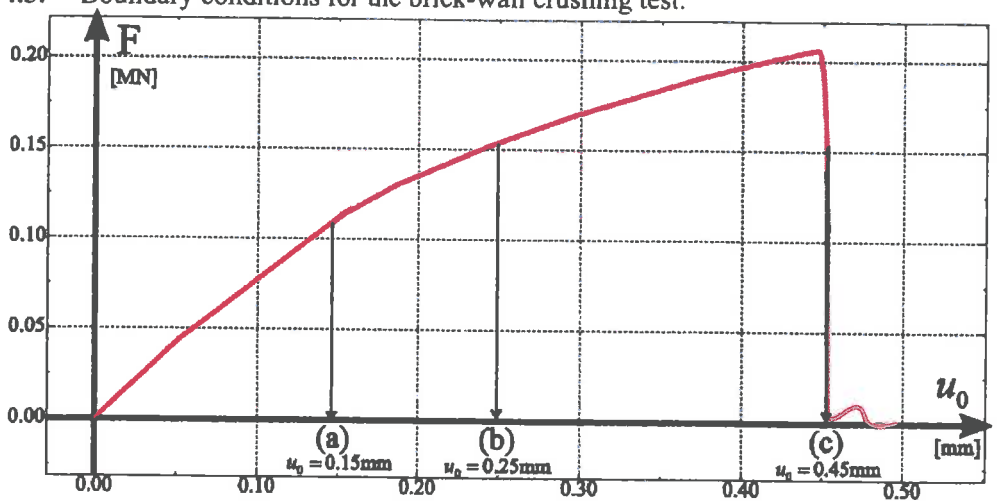


**Figure 4.4.** The total reaction force as a function of displacement applied on the CD edge in masonry wall subjected to compression loading.

Fig 4.4 presents the response of the masonry wall subjected to compression loading (as a summary reaction to the applied on the CD edge displacement boundary conditions). On that graph the characteristic values of the absolute displacement on CD boundary, for which the following contour graph are made, are marked as (a), (b) and (c). Finally Fig 4.5 shows the contour graphs of Mises stress in the model in three phases of the load (cf. Fig. 4.4). Figures 4.6 and 4.7 show maximal principal plastic strain and interface damage initiation criterion (2.4) respectively.

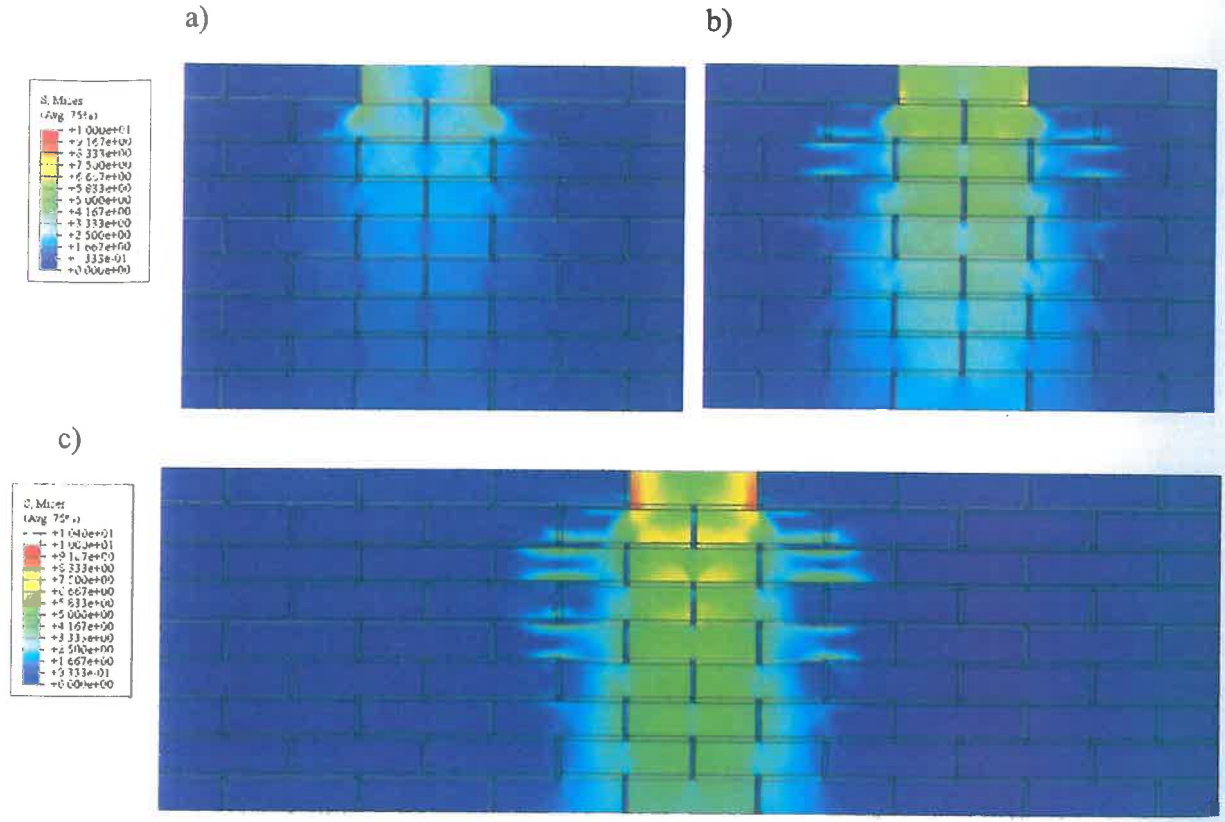


**Figure 4.5.** Mises stress in the model when maximal displacement is: a): 0.15 mm, b): 0.25 mm , c): 0.45 mm.

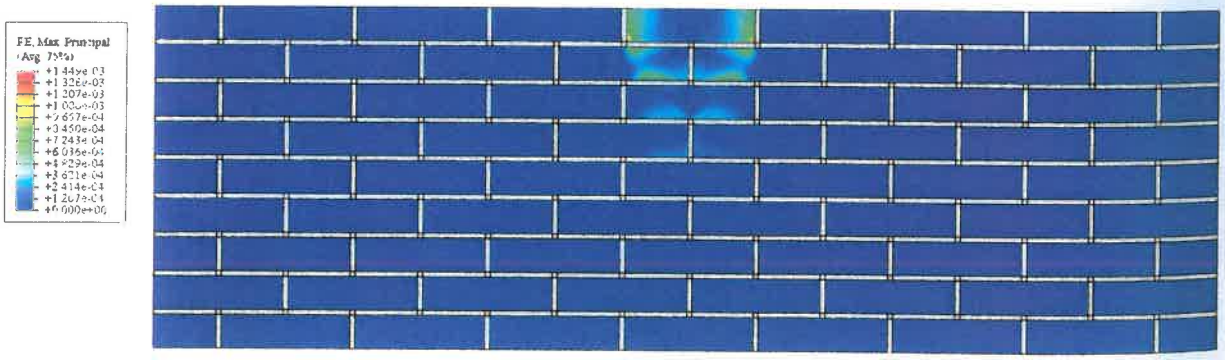

**Figure 4.6.** Plastic strain in the model when maximal displacement is equal to 0.45 mm (c).

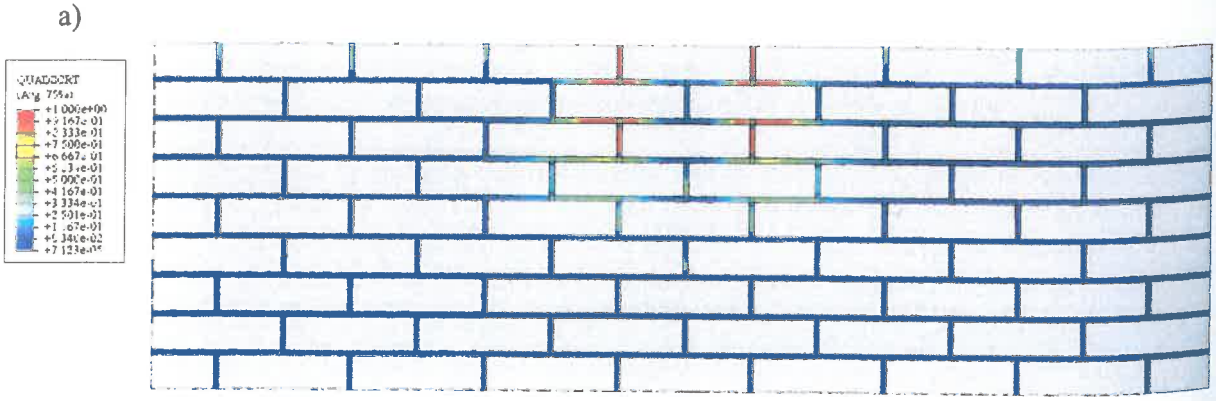

b)

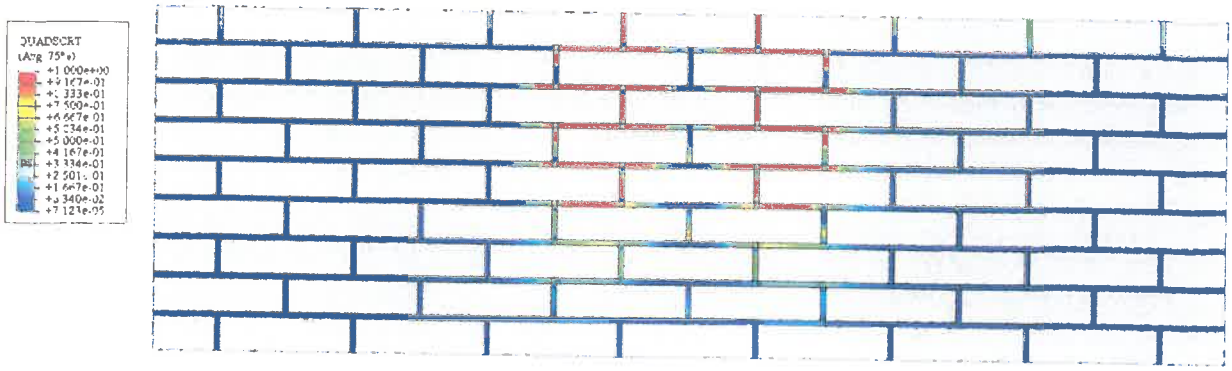

c)

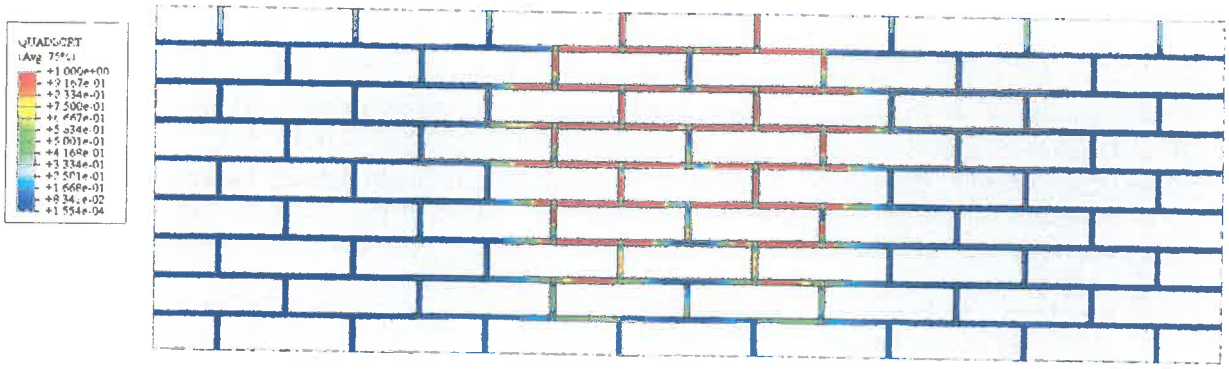

**Figure 4.7.** Damage initiation criterion when maximal displacement is equal to: a): 0.15 mm, b): 0.25 mm, c): 0.45 mm.

## 5. Final remarks and general conclusions

The walls of the buildings are designed in a way to reduce the incidence of a locally significant tensile stresses. The specificity of these structures leads to observations which indicate that the typical failure mechanism is in most cases initiated in the mortar interface as a result of shearing and relatively small tension. An approach presented in this chapter for the formulation of these types of problems, e.g. constitutive modeling of mortar interfaces with condition for cracks initiation and its further propagation (using also the so-called cohesive finite elements) and modeling of the bricks as an elastic material, is in most cases sufficient, cf. the results presented in Section 3. The use of this method of analysis, in the context of modeling of the experimental tests carried out on the compression/tension of brick panels by Page, leads to qualitatively correct results in all cases of interface (bed joints) orientation with respect to the support when an angle differs from $\theta = 0.0^o$ and $\theta = 90.0^o$. In these two cases the constraint on compression should decide about the fracture of the panel, but no such constraint is included in the model. Accordingly, in Section 4 the extended constitutive model for bricks, with yield condition limiting the brick compressive strength, is proposed. Because in modeling of spatial masonry elements the plane stress assumption was adopted, the simplest possible plasticity yield condition H-M-H was used and its parameters were chosen so that it complies with uniaxial and biaxial compression. This condition was also modified by the inclusion of isotropic strain hardening/weakening. In case of bricks the typical brittle materials relationship between the stress and strain state was assumed (e.g. after crack initiation a slight hardening takes place, after which constant weakening of the material occurs, until complete failure). For such re-formulated constitutive model the numerical

solutions to the problem of panel compression/tension tests for $\theta = 0.0^o$ and $\theta = 90.0^o$ were found again. Thanks to that re-formulated constitutive model, it was possible to determine limitation for the failure surface shown in Fig. 3.3 in the region of dominant compressive stresses (see. Fig. 4.2). Such formulated model was successfully used to solve a problem of compressive crushing of nine-layer brick wall.

However, it seems that further theoretical studies on the constitutive model of interface between masonry components, that would take into account the restriction of compressive stress in the mortar layer as well, should be carried out, since, depending on the relative compression strength of the mortar and brick, the initiation of the failure due to compression may be present in both elements.

## Bibliography


[1] Abaqus Theory Manual, Version 6.11, Dassault Systèmes, Abaqus, 2011.

[2] Bilko P.: Numerical analysis of the masonry failure mechanisms, Phd, Warsaw University of Technology, Warsaw, 2013 (in polish).

[3] Camanho P. P., Dávila C. G.: Mixed-Mode Decohesion Finite Elements for the Simulation of Delamination In Composite Materials, NASA/TM-2002-211737, pp. 1-37, 2002.

[4] Dhanasekar M., Page A.W., Kleeman P.W.: The failure of brick masonry under biaxial stresses, Proceedings from the Institution of Civil Engineers - Part 2, 79, pp. 295–313, 1985.

[5] Gajewski M., Jemioło S.: On cohesive element application in analysis of masonry structures, Logistyka, 6, 2010 (in polish).

[6] Jemioło S., Małyszko L., FEM and constitutive modeling in masonry failure analysis, UWM Publishing House, Olsztyn, 2013 (in polish).

[7] Kowalewski Ł., Gajewski M.: Determination of failure modes in brick walls using cohesive elements approach, Procedia Engineering, vol. 111, pp. 454–461, 2015.

[8] Lourenço P. B., Rots J. G., Blaauwendraad J.: Two Approaches for the Analysis of Masonry Structures: Micro-and Macro-Modeling, Heron, Vol. 40, No. 4, pp. 313-340, 1995.

[9] Lourenço P. B.: Computational strategies for masonry structures, Phd, Delft University of Technology, The Netherlands, Delft, 1996.

[10] Lubliner J.: Plasticity theory. Macmillan Publishing Company, New York, 1990.

[11] Małyszko L.: Modelling of failure in masonry structures taking into account its anisotropic properties, Dissertations and monographs of University of Warmia and Mazury, 105, UWM Publishing House, Olsztyn, 2005 (in polish).

[12] Małyszko L., Jemioło S., Bilko P., Gajewski M.: FEM and constitutive modeling in masonry failure analysis, Implementations and examples, UWM Publishing House, Olsztyn, 2015 (in polish).

[13] Page A. W.: The strength of brick masonry under biaxial tension-compression, Proceedings from the Institution of Civil Engineers - Part 2, 71, pp. 893-906, 1981.

[14] Page A. W.: The biaxial compressive strength of brick masonry, International journal of masonry constructions, 3(1):26-31, 1983.

[15] Van der Pluijm R.: Non-linear behavior of masonry under tension, Heron, vol. 42, No. 1, pp. 25-54, 1997.

Publications of the Warsaw University of Technology Publishing House (OWPW — Oficyna Wydawnicza Politechniki Warszawskiej) and its publication catalogues are available in most technical-scientific bookshops in Poland, as well as in reading rooms and libraries of universities.

The full offer of our publications is presented on the Internet at:

www.wydawnictwopw.pl

The Warsaw University of Technology Publishing House offers also mail-order sale (national and international deliveries):

- phone (48) 22-234-75-03
- fax (48) 22-234-70-60
- e-mail oficyna@pw.edu.pl

ISBN 978-83-7814-607-0